

Received May 1, 2019, accepted May 31, 2019, date of publication June 5, 2019, date of current version July 17, 2019.

Digital Object Identifier 10.1109/ACCESS.2019.2920944

The Effect of Tidal Geoelectric Fields on GIC and PSP in Buried Pipelines

LIANGUANG LIU^{1,2}, ZEBANG YU¹, XUAN WANG¹, AND WENLIN LIU²

¹State Key Laboratory of Alternate Electrical Power System with Renewable Energy Sources, North China Electric Power University, Beijing 102206, China

²Dezhou Tianhe Benan Electric Power Technology Co., Ltd., Dezhou 253000, China

Corresponding author: Zebang Yu (yuzebang@126.com)

This work was supported by the National Key R and D Program of China under Grant 2016YFC0800100, the National Natural Science Foundation of China under Grant 51577060 and the Fundamental Research Funds for the Central Universities under Grant 2018QN018.

ABSTRACT Compared with the investigation of geomagnetically induced currents (GIC) in power grids, there is less study about the effect of geomagnetic disturbance (GMD) on buried oil and gas pipelines in mid-low latitude areas, which includes GIC and pipe-to-soil potentials (PSP) effects. Therefore, it is of great significance to research the GMD effect in the mid-low latitudes. For this purpose, we performed the observation experiments on GMD influencing the GIC and PSP in China's oil and gas pipelines. The data of GIC and PSP in the pipelines are obtained, which do not pertain to the characteristics of the geomagnetic storms caused by solar activity, as well as the GIC and PSP monitoring data deriving from geomagnetic storm on May 21, 2016. By analyzing the characteristics of waveform, frequency and phase of the geoelectric fields data from Lingyang Geomagnetic Observatory (35°32'N, 118°52'E) 60 km away in northeast from the pipeline observation site, the study corroborated that GIC and PSP variations are driven by tidal geoelectric fields (TGF) during the geomagnetic quiet days in this paper. The mechanism of GIC generated by tidal geoelectric field is analyzed. Likewise, an analysis of GMD data from the Maling Mountain Geomagnetic Observatory (34°42'N, 118°27'E), the GIC and the PSP have been done, it is illustrated that the GIC and PSP effects are caused by TGF and geomagnetic storm induced geoelectric field together during a geomagnetic storm. The results demonstrated that, near large areas of water, the effect of tidal geoelectric field on pipeline corrosion is persistent and serious. TGF impacts the calculation accuracy of GIC in pipelines and PSP. Therefore, we should account for the errors caused by TGF when calculating GIC and PSP in pipelines near seashores and a large body of water.

INDEX TERMS Electromagnetic interference, Petroleum industry, Geomagnetism, Magnetolectric effects, Corrosion.

I. INTRODUCTION

With the rapid development of the scale of technical systems such as power grids, oil-gas pipelines and railways, the influence and protection of electromagnetic interference on these systems have become an important research topic [1]–[3], among which the influence of geomagnetic disturbances (GMD) caused by geomagnetic storms is a frontier issue [4], [5].

At the high latitudes, such as, North America and Scandinavia, the amplitude of GMDs induced by magnetic storms is commensurate higher. Therefore, the investigation on the effect of geomagnetic induced current (GIC) and the pipe-soil

potentials (PSP) produced by geomagnetic storm on underground pipelines have been carried on earlier there, many experimental results have been obtained [6]–[9]. Boteler et al. have established the theoretical calculation model of pipeline using the distributed source transmission line (DSTL) theory, hence the distribution rule of the GIC and PSP are obtained [10]–[14].

The conclusions of the research in the direct driving sources of geoelectric field and GIC in pipelines shows that the GMD in high latitude areas is related to auroral electrojet. Therefore, the intensity of GMD generated by solar activity is large near the Antarctica and Arctic. Accordingly, the interference of GMD in pipelines and other ground technology systems is a massive problem at high latitudes [15]–[17]. Furthermore, there is no exact explanation for the large

The associate editor coordinating the review of this manuscript and approving it for publication was Wenjie Feng.

fluctuation of GIC in pipelines of some regions when the solar wind activity is weak.

Compared with the high latitudes, the GMD in the middle and low latitudes is weaker. So the research on GIC of pipeline generated by geomagnetic storms is carried out relatively late in China. However, the geoelectric structure of China is complicated, the investigations of the impact of GMD on power grid system demonstrate that GIC has a great impact on China's power systems, the smaller the DC resistance of the conductor is, the larger the GIC in the power grid generated by the GMD will be; the higher the voltage level is, the greater the risk of power grid will be [18]–[20]. With the scale of oil and gas pipelines rapidly increasing in China, the resistance of pipelines decreases because the diameter of pipelines increases. In addition, accompanied by the integrated energy system putting forward in recent years [21]–[24], requirements for the safety of pipeline operation is becoming higher and higher. Thus, the effect of GMD on buried pipelines has become an extremely important research topic in China.

To provide a basis for investigating the corrosion effect of geomagnetic storms and making protection decision, we have carried out an observation experiment for GIC and PSP in pipelines of Shandong Province of China in 2016. Through the data analysis, the GIC and PSP data that do not conform to the characteristics of geomagnetic storms in a coastal oil pipeline have been found firstly, the same disturbance is also found at other observation sites near the seaside. The geoelectric field data obtained by Lingyang Geomagnetic Observatory (35°32'N, 118°52'E) at the geomagnetic quiet time, which is 60 km away in northwest of the oil pipeline, are used to elucidate that the GIC and PSP offset during the geomagnetic quiet period are caused by tidal geoelectric fields (TGF). Furthermore, the geomagnetic field data of Maling Mountain Geomagnetic Observatory (34°42'N, 118°27'E) which is 137 km southwest of the observation site are acquired to illustrate that the TGF impacts the calculation accuracy of the geoelectric field under the geomagnetic storm.

II. COLLECTION OF GEOELECTRIC FIELD DATA

Firstly, in order to illustrate the characteristics difference of the GIC and PSP in coastal pipeline and inland geoelectric field, the geoelectric field data obtained by geomagnetic observatories in inland China are collected.

The geoelectric field of different latitudes in China is measured by Meridian Engineering Data Center using the geoelectric field meters since 2010. The geoelectric observatorion sites are Nongan Observatory, Jiufeng Observatory, Manzhouli Observatory, Pixian Observatory, Zhaoqing Observatory. The locations of these observatories are shown in Fig. 1. The geoelectric field data monitored by these Observatories is shown in Fig. 2, the temporal resolution is 1 minute, the horizontal ordinates are unified to the universal time (UT).



FIGURE 1. The locations of Nongan Observatory, Jiufeng Observatory, Manzhouli Observatory, Pixian Observatory, Zhaoqing Observatory, Maling Mountain Observatory and Rizhao City.

III. OBSERVATION SCHEMES OF GIC AND PSP OF BURIED PIPELINES

A. GIC FLOW PATH IN PIPELINE

In order to restrain the corrosion caused by stray current, insulated coating and grounding resistance for drainage are usually installed in the buried pipeline. The standard stipulates that the resistivity of the insulating coating is not less than $10000\Omega \cdot \text{m}^2$ [25], so the coating can be regarded as the large resistance. The induced electric field of pipeline which related to the rate of change in geomagnetic field creates a GIC through the closed loop composed of pipeline steel wall, insulating coating, coating defect and grounding device. Majority of GIC flows into the ground from coating defects, which increases the current density and causes corrosion at the defects. The potentiostat in the cathodic protection station outputs a current to pipeline, which can compensate the GIC according to the offset of PSP. The flow path of pipeline current is shown in Fig. 3.

B. OBSERVATION SCHEME OF PIPELINE

As shown in Fig. 3, there are two kinds of current components in the pipeline, one of them is the compensation current (I_c) output by the potentiostat, the other is the GIC. To monitor the GIC, I_c and the current flowing in the pipeline (I_p) need to be measured simultaneously. GIC can be expressed as $I_G = I_p - I_c$. The magnitude of GIC and PSP offset can reflect the corrosion situation of pipeline. In view of the difficulty of installing the monitor in buried pipelines, two Hall sensors have used to synchronously measure the I_c and the current in jumper wire in the cathodic protection station. The current

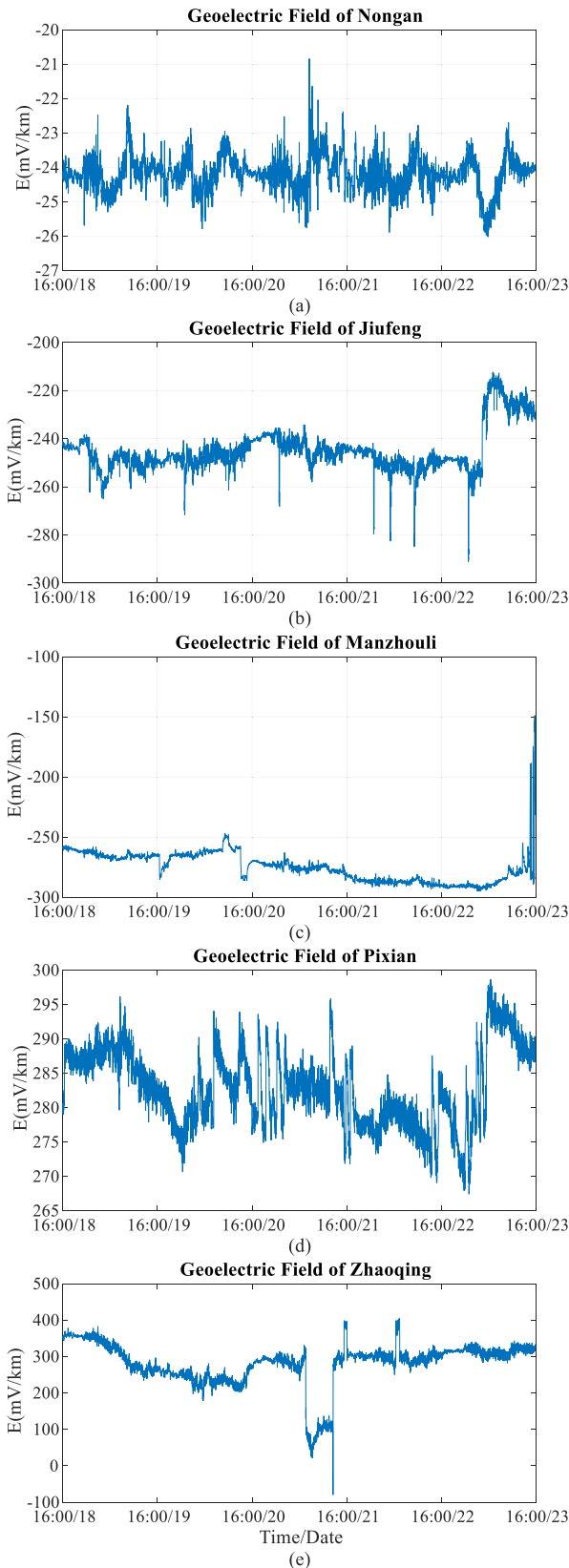


FIGURE 2. The monitoring results of the geoelectric field monitored by the Observatories from May 18th to 23th, 2016.

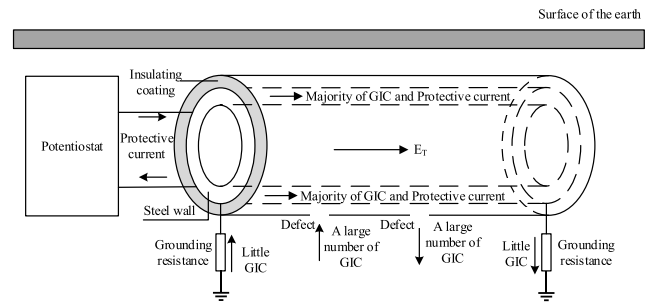


FIGURE 3. GIC flow path of Pipeline with defects and potentiostat.

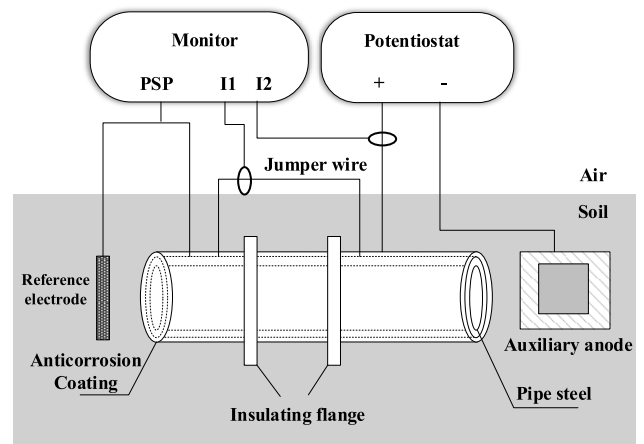


FIGURE 4. The structure diagrammatic sketch of the cathodic protection station and the installation of the GIC-PSP monitor.

in the jumper wire is equal to I_p as shown in Fig. 4. At the same time, Hall voltage sensor is installed to detect the PSP. The structure diagrammatic sketch of the cathodic protection station and the installation of the GIC-PSP monitor is shown in Fig. 4.

Rizhao City is located at the seaside. Because the coast effect of geomagnetic storms and the influence of tides, the pipeline in this area is seriously disturbed by geomagnetic field. A cathodic protection station ($35^{\circ}06'N$, $119^{\circ}22'E$) of an oil pipeline in Rizhao City has been chosen as an observation site. The pipeline starts from Rizhao City and ends in Heze City in Shandong Province as shown in Fig. 5. After laboratory testing, the GIC-PSP monitor is installed and commissioned in May 2016.

IV. DATA ANALYSIS

According to the report of the Chinese Academy of Sciences Space Environment Research and Prediction Center, at 04:00 to 13:00 on May 21, 2016, a geomagnetic storm event with $K_p = 5$ occurred. The data acquired from the Rizhao observation site are analyzed. The results indicate that the magnitude and variation characteristics of the GIC and PSP show low correlation with the characteristics of



FIGURE 5. The path of the monitoring pipeline in Shandong Province.

the geoelectric field during geomagnetic storms observed by majority Geomagnetic Observatories. In order to ascertain the driven source of the GIC, we have gathered the data of PSP, GIC and the geoelectric field in Lingyang Geomagnetic Observatory on 19 ~ 23 May. Fig. 6 (a), (b) and (c) respectively shows the East-West component of geoelectric field in Lingyang (the positive direction is west), the GIC in the pipeline (the positive direction is west), the PSP and the tidal force. Comparing the geoelectric data shown in Fig. 2 and the Fig. 6, it can be seen that the characteristics of the geoelectric data of inland Observatories is different from that of the GIC and the PSP in Rizhao pipelines.

A. THE DRIVEN SOURCE OF GIC IN GEOMAGNETIC QUIET PERIOD

The Fig. 6 illustrated that the waveform characteristic of GIC and PSP is almost the same as that of East-West component of geoelectric field in Lingyang. Ignoring the variation of the data in geomagnetic storm period (04:00 ~ 13:00 May 21), all of the curves conform to the law of approximate sinusoidal periodic fluctuation. The correlation coefficient between East-West component of geoelectric field and GIC, PSP are respectively 0.75 and 0.81, which can be calculated by the formula as follow:

$$r = \frac{\text{cov}(A, B)}{\sigma_A \sigma_B} \tag{1}$$

The $\text{cov}(A, B)$ is the covariance of A and B , σ_A is the standard deviation of A , σ_B is the standard deviation of B . GIC and PSP are apparently driven by the geoelectric field with approximate sinusoidal periodic properties.

Dacheng Tan *et al.* have researched in the mechanism of the generation of tidal geoelectric field [26]–[28]. The results show that the type-A tidal geoelectric field (TGF-A) is generated by the alteration of cranny water periodic transfusion in the rock due to stress change. At the same time, the theory of tidal generator indicates that the B-type tidal geoelectric field (TGF-B) is closely relate to the S_q current produced by air tide. It generates induced electric field on the surface of the earth. Under the action of TGF, an induced electric field is generated in the buried pipeline, it causes the GIC through a closed loop formed by steel wall of pipeline, insulation

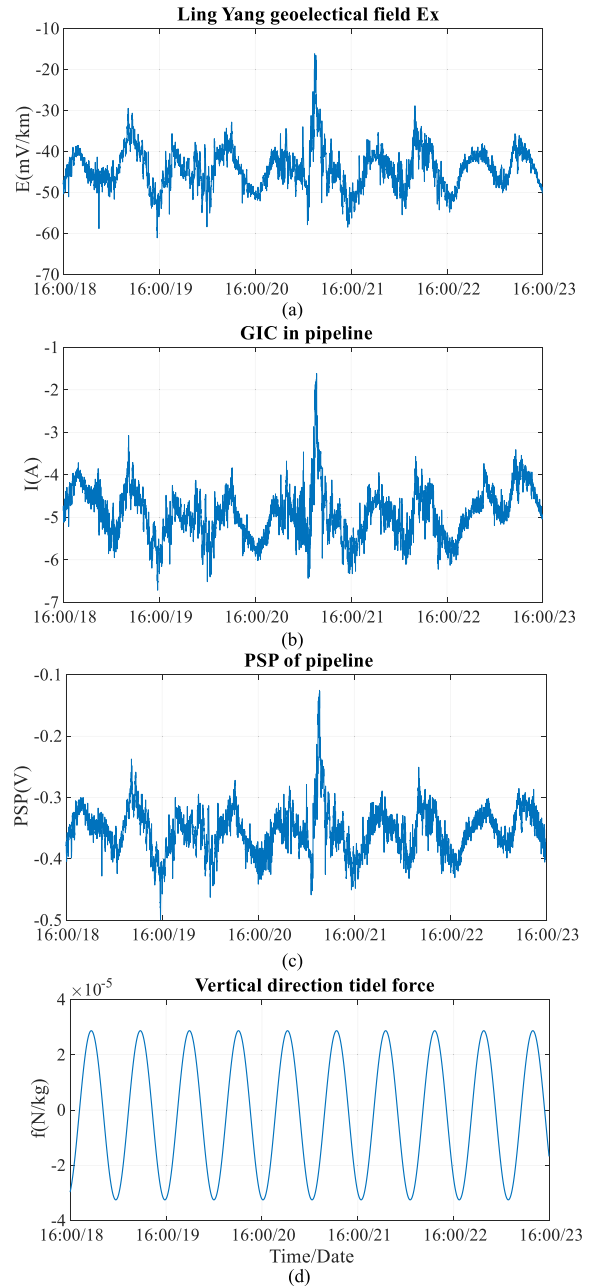


FIGURE 6. (a) East-West component (Ex) of the geoelectric field of Lingyang Geomagnetic Observatory, (b) GIC and (c) PSP of pipeline in Rizhao site on 19 ~ 23 2016(UT), (d) tidal force calculation result.

coating, coating defect and pipeline grounding electrode, this mechanism process is shown in Fig. 7.

According to previous statistical data of more than 100 Geomagnetic Observatories, TGF-A basically distribute near the large area of water, elucidated that the curves of TGF-A changed approximately with stable sinusoidal fluctuations near the large body of water in China [26]. Lingyang Geomagnetic Observatory and Rizhao city are located at the seaside, their hydrological factors satisfy the formation conditions of TGF-A. The waveform characteristic of the

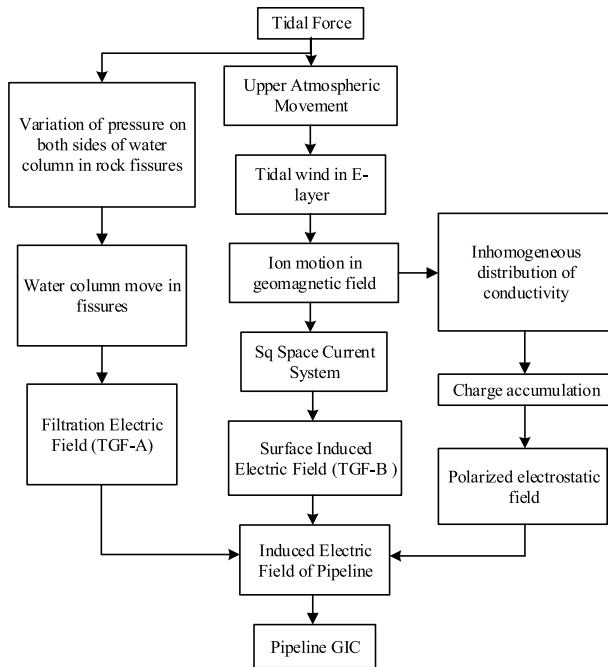


FIGURE 7. The mechanism of the tidal force affecting the buried pipeline.

Linyang geoelectric field, GIC and PSP in Rzhao pipeline is same to that of TGF-A. TGF-B widely distributes in areas with high water content and good permeability, it presents approximate trapezoidal waves because its variation amplitude around noon conforms to the approximate sine law and there is less variation in other phases of a day, the geoelectric field data of Nongan Station, as shown in Fig. 2(a), can be regarded as a typical TGF-B. By considering the possible influences on pipelines such as the hydrological conditions of Rizhao and the artificial technology systems including mine electric traction train and power transmission system, it is preliminarily identified that the variations of GIC and PSP of the Rizhao pipeline are driven by the TGF-A during the geomagnetic quiet period. In order to prove this inference, the analysis of the frequency characteristic and the phase characteristic of TGF-A as well as the observation data are made as follow.

B. FREQUENCY CHARACTERISTIC ANALYSIS

The research results in [26] showed that the frequency of the first and the second order harmonic with strongest TGF-A amplitude belong to the collection 1.2×10^{-5} Hz, 2.3×10^{-5} Hz, 3.5×10^{-5} Hz, 4.6×10^{-5} Hz and 5.8×10^{-5} Hz. Using the discrete Fourier transform, the spectrum diagram of the East-West components of Linyang geoelectric field is obtained as shown in Fig. 8, which indicated that the first two order harmonic frequency with the strongest amplitude is 2.3×10^{-5} Hz and 1.2×10^{-5} Hz respectively. This results reveals that the frequency characteristic of geoelectric field in Linyang is coincide with that of TGF-A.

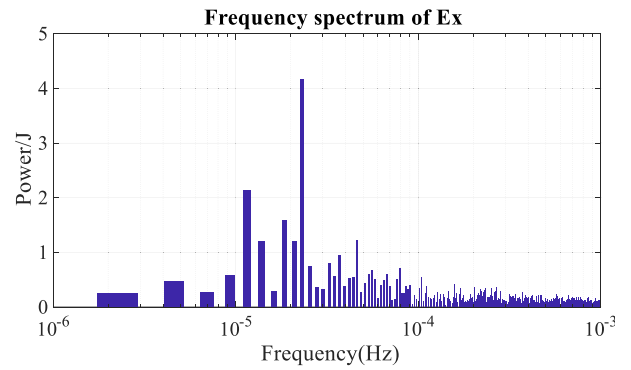


FIGURE 8. The spectrum diagram of the geoelectric field East-West component in Linyang on May19-23, 2016.

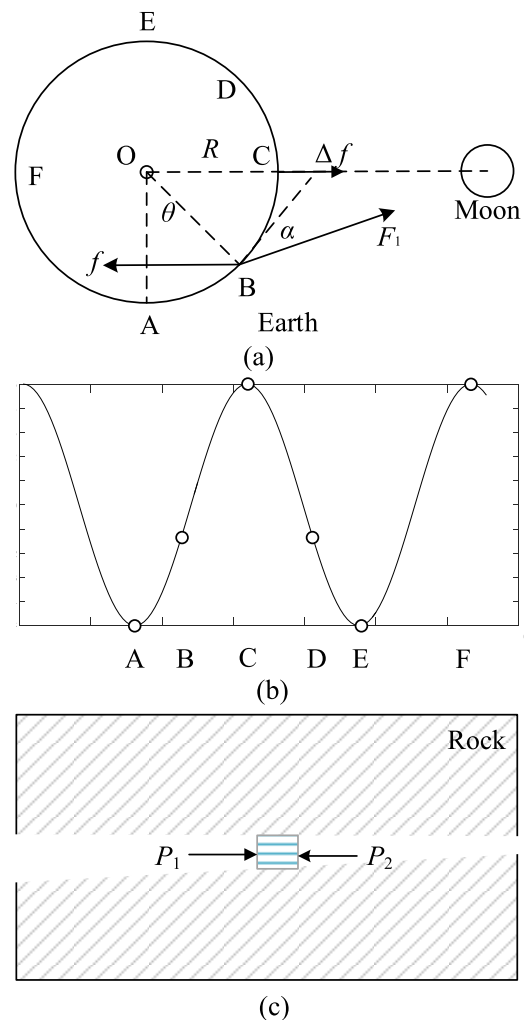


FIGURE 9. The sketch of the formation of tidal force.

C. PHASE CHARACTERISTIC ANALYSIS

With the relative motion of the Earth and the Moon, the tidal force (Δf) of a particle on the Earth varies at different time, as shown in Fig. 9 (a). When the particle moves to A or E, Δf is the smallest. When it moves to C or F, Δf is the largest.

When it moves to B or D, Δf is parallel to the surface of the Earth. Therefore, the amplitude of Δf presents an approximate sinusoidal variation in low and middle latitudes as shown in Fig. 9 (b). Rock fissure flow pipes near large areas of water are connected with the water area as shown in Fig. 9 (c). There are a large number of water columns in the pipes, the fissure water percolates for a long time and subjects to the common pressure of the water area and air in the fissure. It is assumed that the pressure on both sides of the water columns is P_1 and P_2 respectively. The pressure difference ($\Delta P = P_1 - P_2$) follows the variation of the Δf . According to the analysis of Fuye Qian *et. al.*, the driving force of seepage process mainly is ΔP [29]. The current velocity (q_r) of the solution in the rock fissure depends on the pressure difference (ΔP) and the viscosity coefficient (μ) of the solution, its expression can be written as [30]:

$$q_r = \frac{dP}{4\mu dx} (r_0^2 - r^2) \approx \frac{r \Delta r dP}{2\mu dx} \quad (2)$$

r is the distance between the center of rock fissure and the compact layer, r_0 is the distance between the center of rock fissure and the negative ion layer (the wall of the fissure), $\Delta r = r_0 - r$ is the thickness of the electric dipole layer (the distance between the capacitor polar plates). The positive direction of x in the equation is the direction of the liquid flow.

If the rock fissure in Fig. 9 (c) is approximately regarded as a charged cylindrical capacitor, the electric quantity Q of per unit length of the capacitor can be expressed as [30]:

$$Q = C \Delta u \quad (3)$$

$$C = \frac{2\pi \epsilon_0 \epsilon}{\ln \frac{r_0}{r}} = \frac{2\pi \epsilon_0 \epsilon}{\ln \frac{r+\Delta r}{r}} = \frac{2\pi \epsilon_0 \epsilon}{\ln(1 + \frac{\Delta r}{r})} \approx \frac{2\pi \epsilon_0 \epsilon r}{\Delta r} \quad (4)$$

$$Q = \frac{2\pi \epsilon_0 \epsilon r \Delta u}{\Delta r} \quad (5)$$

C is the capacitance of a cylindrical capacitor, Δu is the potential difference of the electric dipole layer (the potential difference between the two polar plates of the capacitor), ϵ is the dielectric constant of the medium, ϵ_0 is the vacuum dielectric constant.

Thus, the current (I) whose direction is opposite to the direction of liquid flow is [30]:

$$I = Qq_r = \frac{\pi \epsilon_0 \epsilon r^2 \Delta u}{\mu} \frac{dP}{dx} \quad (6)$$

The current density (J) is:

$$J = \frac{I}{\pi r^2} = \frac{\epsilon_0 \epsilon \Delta u}{\mu} \frac{dP}{dx} \quad (7)$$

Because $J = E_0/\rho$, the filtering electric field E_0 can be calculated as [30]:

$$E_0 = \frac{\epsilon_0 \epsilon \rho \Delta u}{\mu} \frac{dP}{dx} \quad (8)$$

ρ is the resistivity of the solution. The filter potential (u) can be calculated by the integral of the formula (8):

$$u = -\frac{\epsilon_0 \epsilon \rho \Delta u}{\mu} P \quad (9)$$

Thus, Δu can be obtained as follow:

$$\Delta u = k \frac{\rho}{\mu} \Delta P \quad (10)$$

$k = \epsilon_0 \epsilon \Delta \mu$. k can be obtained by experimental method. For general rocks, $k \approx 0.77$ [30]. At 20° , the formula (10) can be simplified as follows:

$$u = 0.77 \times \rho \times \Delta P \quad (11)$$

The filtering electric field (E) observed on the ground is related to the properties of the upper and lower rock stratum of the filter layer. It is supposed that the filter layer is covered with conductive layer with resistivity of ρ_1 and thickness of h_1 , the resistivity of the filter layer is ρ_2 and thickness of h_2 . Underneath the filter layer is nonconductive rock. The expressions of E is as follow [30]:

$$E = \frac{S_2}{S} E_0 \quad (12)$$

E_0 is the filter electric field without covering layer, μ_0 is the potential at $x = 0$, $S_2 = h_2/\rho_2$ is the longitudinal conductance of the filter layer, $S = h_1/\rho_1 + h_2/\rho_2$ is the longitudinal conductance of the layer combined by filter layer and the cover layer.

When ρ_1 , h_1 , ρ_2 and h_2 are unchanged, E is proportional to E_0 . The E_0 follows the variation of Δu , so the E follows the variation of the ΔP . In other words, the E follows the variation of the Δf .

In Fig. 9 (a), the particle (Δm) on the meridional plane of the earth is acted by both the gravitational force (F_1) of the Moon and the inertial centrifugal force (f). The mass of the moon (without considering the radius) is M , the radius of the Earth is R , the distance between the Moon and the Earth is $60.3R$, the gravitational constant is G . The angle θ and α are shown in Fig. 9 (a), in which θ ranges from 0° to 360° and α from 0° to 90° . In order to solve the tidal force Δf , the deductions can be made as following [27]:

$$\begin{aligned} \Delta f &= F \sin \alpha - f \sin \theta \\ &= \frac{G \Delta m M}{R^2(60.3^2 - 120.6 \sin \theta + 1)} \sin \alpha \\ &\quad - \frac{G \Delta m M}{R^2 60.3^2} \sin \theta \end{aligned} \quad (13)$$

According to the geometric relationship in Fig.9 (a), we can see that:

$$\sin \alpha = \frac{60.3 \sin \theta - 1}{(60.3^2 - 120.6 \sin \theta + 1)^{1/2}} \quad (14)$$

the tidal force Δf can be written as:

$$\Delta f = \frac{\Delta m M G}{R^2} \left[\frac{60.3 \sin \theta - 1}{(60.3^2 - 120.6 \sin \theta + 1)^{3/2}} - \frac{\sin \theta}{60.3^2} \right] \quad (15)$$

$M = 7.35 \times 10^{22}$ kg, $R = 6.37814 \times 10^6$ m, $G = 6.67259 \times 10^{-11}$ N · m² · kg⁻² [23]. According to the phase statistics of the lunar, the angle θ between the particle and the OA at 16:00 on May 18, 2016 is about 26.9218° [31].

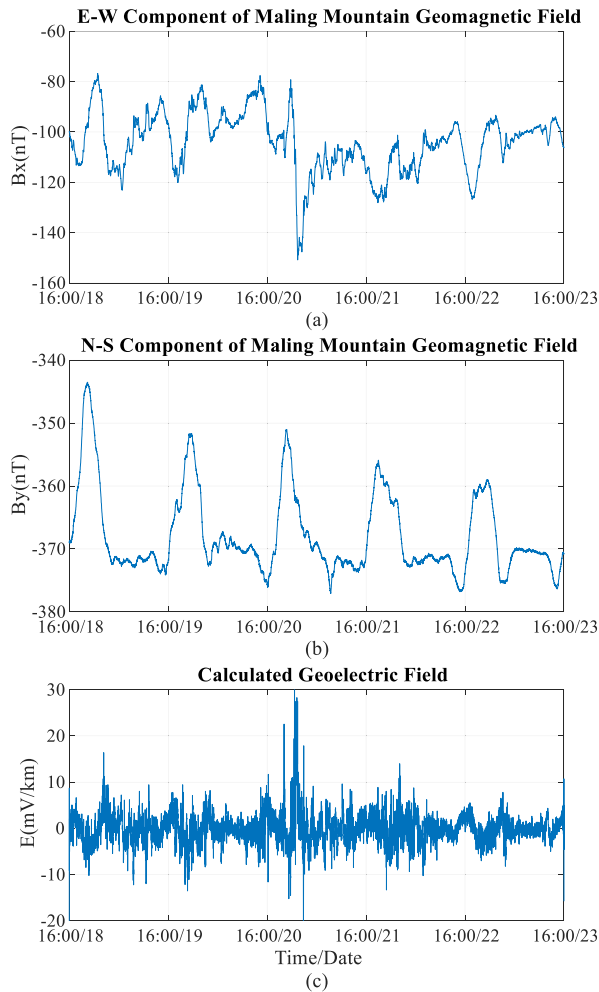


FIGURE 10. The geomagnetic horizontal components B_x (a) and B_y (b), the calculation result of the geoelectric field (c) from May 18th to 23th, 2016.

The tidal force of Rizhao calculated using (15) is shown in Fig. 6 (d). The occurrence time and the value of the crest and trough of tidal force Δf , Lingyang geoelectric field E , GIC and PSP are shown in Table 1. It can be seen that the occurrence time of tidal force have a good correlation with that of Lingyang geoelectric field, pipeline GIC and PSP. The deviation between 04:00 and 13:00 on May 21 are caused by geomagnetic storms.

In summary, the characteristic of waveform, frequency and phase of GIC and PSP obtained from the observation site in Rizhao are basically consistent with the characteristic of TGF-A. Therefore, the GIC and PSP offsets of pipelines in Rizhao area during geomagnetic quiet period are driven by TGF-A.

V. INFLUENCE OF TGF ON GIC AND PSP

A. MAGNITUDE ANALYSIS OF GIC AND PSP PRODUCED BY TGF-A

As shown in Fig. 6 (b), the GIC of observation site caused by TGF-A reaches the trough at 16:00 daily and then rises

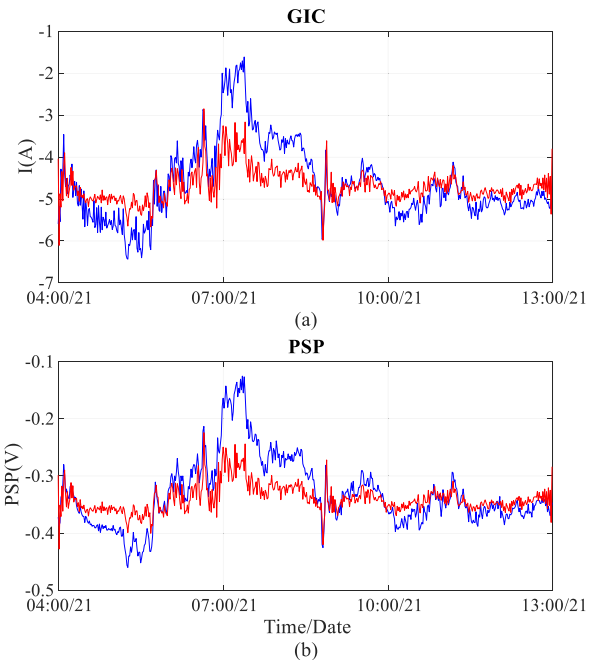


FIGURE 11. The monitoring (blue) and calculation (red) results of the GIC (a) and PSP (b) in pipeline on May 21, 2016.

gradually to crest after about 6 hours, and returns to the trough again about 10:00 next day. The variation in the afternoon is similar to that in the morning. The crest and trough values of GIC in Table 1 indicated that the magnitude of GIC in quiet period ranged from 3.07 A to 6.65 A.

Fig. 6 (c) showed that the curve of the PSP was similar to the one of the GIC. The two sets of data had apparent correlation with coefficient 0.9341. So the fluctuation characteristic of PSP was also consistent with the tidal force. The peak and valley values of PSP in Table 1 showed that the PSP values in quiet period ranged from -0.49V to -0.25V . The Reference [32] stipulates that DC current interference can be confirmed when PSP is positively offset by 20 mV. The drainage or other protective measures must be taken when PSP is positively offset by 100 mV. Fig. 5 shows that the positive offsets of PSP driven by TGF-A can exceed 100 mV. Tidal geoelectric field is a kind of continuous natural electric field, so the pipelines need to take long-term drainage measures to prevent the impact of TGF-A.

B. THE EFFECT OF TGF-A AND GEOMAGNETIC STORMS ON THE PIPELINE

Because the influence of geomagnetic storm is global, in another words, GIC and PSP of the oil and gas pipeline network all over the world will respond to the geomagnetic storm when it occurs. The influence of TGF-A is concentrated near large body of water. Therefore, the GIC and PSP of Rizhao Pipeline are produced by the interaction of geomagnetic storms and TGF-A during magnetic storms.

In order to compare the contribution of TGF-A and geomagnetic storms to GIC and PSP in pipeline, the monitoring

TABLE 1. The crest and trough and their occurrence time of Δf , E in linyang, GIC and PSP in the pipeline.

Values	Δf 's Time	E 's Time	E (mV/km)	GIC's Time	GIC (A)	PSP's Time	PSP (V)
Crest	18/21:17	18/19:50	-38.58	18/19:50	-11.14	18/19:50	-0.312
Trough	19/03:31	19/03:31	-51.08	19/03:31	-17.84	19/03:31	-0.652
Crest	19/09:17	19/09:17	-29.47	19/09:17	-9.22	19/09:17	-0.144
Trough	19/15:46	19/15:46	-60.85	19/15:46	-19.96	19/15:46	-0.868
Crest	19/21:46	19/21:17	-35.74	19/21:17	-12.74	19/21:17	-0.3
Trough	20/04:00	20/04:00	-58.38	20/04:00	-19.54	20/04:00	-0.778
Crest	20/10:14	20/10:14	-32.82	20/10:14	-11.5	20/10:14	-0.216
Trough	20/16:43	20/16:43	-51.83	20/16:43	-18.04	20/16:43	-0.7
Crest	20/22:29	20/22:29	-36.03	20/22:29	-12	20/22:29	-0.284
Trough	21/04:29	21/04:29	-57.31	21/04:29	-19.3	21/04:29	-0.776
Crest	21/10:43	21/07:21	-16.54	21/07:21	-4.84	21/07:21	0.22
Trough	21/16:43	21/15:13	-57.73	21/15:13	-18.96	21/15:13	-0.752
Crest	21/22:29	21/22:29	-37.24	21/22:29	-12.1	21/22:29	-0.296
Trough	22/05:29	22/05:41	-53.95	22/05:41	-18.32	22/05:41	-0.696
Crest	22/11:43	22/09:19	-28.58	22/09:19	-11.6	22/09:19	-0.152
Trough	22/17:30	22/17:30	-54.04	22/17:30	-18.26	22/17:30	-0.652
Crest	22/23:26	23/01:07	-39.86	23/01:07	-11.2	23/01:07	-0.312
Trough	23/05:55	23/05:55	-50.09	23/05:55	-15.4	23/05:55	-0.596
Crest	23/11:55	23/11:55	-36.27	23/11:55	-11.2	23/11:55	-0.312

Δf 's Time, E 's Time, GIC's Time and PSP's Time means the occurrence time of the Crest and Trough of tidal force, geoelectric field, GIC and PSP. E (mV/km), GIC (A) and PSP (V) means the value of the Crest and Trough of geoelectric field, GIC and PSP.

TABLE 2. Ground stratified structure of maling mountain & rizhao.

Deep/km	Resistivity/ $\Omega \cdot m$
0-50	2000-10000
50-120	500-2000
>120	50-500

data of Maling Mountain Magnetic Observatory are selected as a reference. As shown in Fig. 1, Maling Mountain is farther from the coastline compared to Linyang, the distance between Maling Mountain and the coastline is about 70 km. Both Maling Mountain and Rizhao are located to the east of Tancheng-Lujiang fracture zone, there is no variation of lateral ground conductivity between them. So it is considered that the geoelectric stratified structure of this two areas are the same as shown in Table 2. Based on the Table 2 and the plane wave theory [33], the geoelectric stratification model of Malingshan area is established. The geomagnetic field data of Maling Mountain Geomagnetic Observatory are used to calculate the geoelectric field of this area from May 18 to 23, 2016, as shown in Fig. 10. Fig. 10 (a) and (b) are respectively the East-West and North-South components of

the geomagnetic field of Maling Mountain, Fig. 10 (c) is the calculated geoelectric field. The results show that the geoelectric field of Maling Mountain area is not effected by TGF-A. By comparing the Fig. 10 (a) and (c), it can be seen that the magnitude of the geoelectric field E is related to the change rate of the E-W component of the geomagnetic field. The larger the decline rate of the geomagnetic field is, the larger the E is, which then drive currents in pipeline.

A GMD caused by geomagnetic storm ($K_p = 5$) occurred at 04:00-13:00 May 21, 2016 (UT). When the effect of TGF-A is neglected, the GIC and PSP of the Rizhao pipeline during 04:00-13:00 May 21, 2016 are calculated according to the DSTL theory and the calculated geoelectric field in Fig. 10 (c). The results are shown as the red waveform in Fig. 11 (a) and (b). In order to obtain the calculation error, the monitoring results of GIC and PSP of Rizhao pipeline in the meantime are provided as shown in Fig. 11 (blue waveform). Comparing the results of calculation and monitoring, it can be seen that, because the GIC during geomagnetic storm is caused by TGF and GMD jointly, neglecting the effect of TGF-A would bring great errors to the calculation results of the GIC and PSP.

According to the data in Table 1, when the geomagnetic storm occurred, the GIC is larger than that during the

geomagnetic quiet period. The GMD of geomagnetic storm make the GIC and PSP reach the peak earlier. The GIC offset from the trough to the peak increased from 2.01 A on May 20 to 4.82 A. the PSP maximum increased from -0.46 V to -0.27 V, and the largest positive offset reached 0.33 V which is beyond the that in geomagnetic quiet period. According to Faraday's law of electrolysis, the corrosion quantity can be written as:

$$M_c = KIt \quad (16)$$

M_c represents the corrosion quantity, K is the electrochemical equivalent, for steel pipelines, its value is 0.6943 g/A·h. I represents the GIC here, t is the actuation duration of the GIC. It can be seen that the corrosion quantity is not only related to the magnitude of GIC, but also to the action time. According to statistics, a geomagnetic storm can last from a few hours to a few days. The geomagnetic-storm day is, on average, no more than 50 days every year for a solar cycle 11 years. In the area effected by TGF, whether it is TGF-A or TGF-B, the geoelectric field produces GIC and PSP offset continuously. Compared with the occasional geomagnetic storms, the TGF can undoubtedly lead to higher corrosion quantity.

VI. CONCLUSION

Through the observation experiments about the impact of geomagnetic storms on oil-gas pipelines, this study discovered that TGF can also cause GIC and PSP in pipelines. The GIC caused by TGF varying from 3.07 A to 6.65 A. The PSP offset derived from TGF exceeded the maximum stipulated by national standard. So the TGF can accelerate the corrosion for pipelines.

During geomagnetic storms, geoelectric field and GIC in pipelines are produced by the superposition effects of geomagnetic storms and tidal geoelectric field. So the geomagnetic storm will bring more serious interference to buried pipelines. However, the previous calculations of the geoelectric field and the GIC did not take the TGF into account, it would impact the calculation results and cause large errors, especially in the areas near the large body of water.

The induced mechanism of TGF is extremely different from that of geomagnetic storms. Although TGF has an effect only in some areas, it is persistent because it affected by the continuous tidal force. The interference range of geomagnetic storms is global, but it arises with accidental, in other words, its cumulative action time is relatively short. In the areas near the large body of water, compared with the geomagnetic storms, the sustained TGF would produce more corrosion quantity. The theoretical calculations of GIC effects caused by TGF in the technology systems such as power grids and the railway systems are scientific issues which need to be studied in the future.

ACKNOWLEDGMENT

The authors appreciate the Institute of Earthquake Forecasting, CEA for providing geoelectric field data, and the Data

Centre of Meridian Space Weather Monitoring Project for providing geomagnetic field data.

REFERENCES

- [1] C. Liu, Y. S. Ganebo, H. Wang, and X. Li, "Geomagnetically induced currents in ethiopia power grid: Calculation and analysis," *IEEE Access*, vol. 6, pp. 64649–64658, 2018.
- [2] S. F. Odenwald, "The feasibility of detecting magnetic storms with smart-phone technology," *IEEE Access*, vol. 6, pp. 43460–43471, 2018.
- [3] C. Liu, X. Wang, C. Lin, and J. Song, "Proximity effects of lateral conductivity variations on geomagnetically induced electric fields," *IEEE Access*, vol. 7, pp. 6240–6248, 2018.
- [4] D. V. Ratnam, T. R. Vishnu, and P. B. S. Harsha, "Ionospheric gradients estimation and analysis of S-band navigation signals for NAVIC system," *IEEE Access*, vol. 6, pp. 66954–66962, 2018.
- [5] K. Zheng, R. J. Pirjola, D. H. Boteler, and L. G. Liu, "Geoelectric fields due to small-scale and large-scale source currents," *IEEE Trans. Power Del.*, vol. 28, no. 1, pp. 442–449, Jan. 2013.
- [6] W. H. Campbell, "Induction of auroral zone electric currents within the Alaska pipeline," *Pure Appl. Geophys.*, vol. 116, no. 6, pp. 1143–1173, Nov. 1978.
- [7] A. Osella, A. Favetto, and E. López, "Currents induced by geomagnetic storms on buried pipelines as a cause of corrosion," *J. Appl. Geophys.*, vol. 38, no. 3, pp. 219–233, Jun. 1998.
- [8] R. Pirjola, A. Viljanen, A. Pulkkinen, and O. Amm, "Space weather risk in power systems and pipelines," *Phys. Chem. Earth, Part C, Sol., Terr. Planet. Sci.*, vol. 25, no. 4, pp. 333–337, 2000.
- [9] P. A. Fernberg, C. Samson, D. H. Boteler, L. Trichtchenko, and P. Larocca, "Earth conductivity structures and their effects on geomagnetic induction in pipelines," *Annales Geophys.*, vol. 25, no. 1, pp. 207–218, 2007.
- [10] D. H. Boteler and M. J. Cookson, "Telluric currents and their effects on pipelines in the cook strait region of New Zealand," *Mater. Perform.*, vol. 25, no. 3, pp. 27–32, 1986.
- [11] D. H. Boteler, "Geomagnetic effects on the pipe-to-soil potentials of a continental pipeline," *Adv. Space Res.*, vol. 26, no. 1, pp. 15–20, 2000.
- [12] A. Pulkkinen, R. Pirjola, D. Boteler, A. Viljanen, and I. Yegorov, "Modelling of space weather effects on pipelines," *J. Appl. Geophys.*, vol. 48, no. 4, pp. 233–256, Dec. 2001.
- [13] D. H. Boteler and L. Trichtchenko, "A common theoretical framework for AC and telluric interference on pipelines," in *Proc. NACE CORROSION*, Jan. 2005, Art. no. 05614.
- [14] D. H. Boteler, "A new versatile method for modelling geomagnetic induction in pipelines," *Geophys. J. Int.*, vol. 193, no. 1, pp. 98–109, Jan. 2013.
- [15] A. Pulkkinen, M. Hesse, S. Habib, L. V. D. Zel, B. Damsky, F. Policelli, D. Fugate, W. Jacobs, and E. Creamer, "Solar shield: Forecasting and mitigating space weather effects on high-voltage power transmission systems," *Natural Hazards*, vol. 53, no. 2, pp. 333–345, 2010.
- [16] H. Vanhamäki, A. Viljanen, R. Pirjola, and O. Amm, "Deriving the geomagnetically induced electric field at the Earth's surface from the time derivative of the vertical magnetic field," *Earth, Planets Space*, vol. 65, no. 9, pp. 997–1006, Sep. 2013.
- [17] L. Liu, X. Ge, W. Zong, Y. Zhou, and M. Liu, "Analysis of the monitoring data of geomagnetic storm interference in the electrification system of a high-speed railway," *Space Weather*, vol. 14, no. 10, pp. 754–763, Oct. 2016.
- [18] C.-M. Liu, L.-G. Liu, and R. Pirjola, "Geomagnetically induced currents in the high-voltage power grid in China," *IEEE Trans. Power Del.*, vol. 24, no. 4, pp. 2368–2374, Oct. 2009.
- [19] C.-M. Liu, L.-G. Liu, R. Pirjola, and Z. Wang, "Calculation of geomagnetically induced currents in mid-to low-latitude power grids based on the plane wave method: A preliminary case study," *Space Weather*, vol. 7, no. 4, pp. 1–9, Apr. 2009.
- [20] L.-G. Liu, K. Wei, and X.-N. Ge, "GIC in future large-scale power grids: An analysis of the problem," *IEEE Electr. Mag.*, vol. 3, no. 4, pp. 52–59, Dec. 2015.
- [21] Z. Ji and X. Huang, "Day-ahead schedule and equilibrium for the coupled electricity and natural gas markets," *IEEE Access*, vol. 6, pp. 27530–27540, 2018.
- [22] S. Fan, Z. Li, J. Wang, L. Piao, and Q. Ai, "Cooperative economic scheduling for multiple energy hubs: A bargaining game theoretic perspective," *IEEE Access*, vol. 6, pp. 27777–27789, 2018.

- [23] Z. Wei, J. Sun, Z. Ma, G. Sun, H. Zang, S. Chen, S. Zhang, and K. W. Cheung, "Chance-constrained coordinated optimization for urban electricity and heat networks," *J. Power Energy Syst.*, vol. 4, no. 4, pp. 399–407, Dec. 2018.
- [24] X. Xing, J. Lin, Y. Song, Y. Zhou, S. Mu, and Q. Hu, "Modeling and operation of the power-to-gas system for renewables integration: A review," *J. Power Energy Syst.*, vol. 4, no. 2, pp. 168–178, Jun. 2018.
- [25] Y. Xiaohong, "Economic analysis of inside and outside coating technology of natural gas transmission pipeline," *Projects Natural Gas*, vol. 21, no. 2, pp. 89–93, 2001.
- [26] D. Tan, J. Zhao, J. Xi, X. Du, and J. Xu, "A study on feature and mechanism of the tidal geoelectrical field," *Chin. J. Geophys.*, vol. 53, no. 3, pp. 544–555, 2010.
- [27] D.-C. Tan, L. Wang, J.-L. Zhao, J.-L. Xi, D.-P. Liu, H. Yu, and J.-Y. Chen, "Influence factors of harmonic waves and directional waveforms for the tidal geoelectrical field," *Chin. J. Geophys.*, vol. 54, no. 7, pp. 470–484, 2011.
- [28] D.-C. Tan, J.-L. Zhao, X.-F. Liu, Y.-Y. Fan, J. Liu, and J.-Y. Chen, "Features of regional variations of the spontaneous field," *Chin. J. Geophys.*, vol. 57, no. 5, pp. 318–331, 2014.
- [29] F.-Y. Qian and Y.-L. Zhao, "Study on geoelectric field method for short-term and impending earthquake prediction," *Earthquake*, vol. 25, no. 2, pp. 33–40, 2005.
- [30] Z. Sun and H. Wang, "Natural electric field," in *Geoelectrical Introduction*. Beijing, China: Seismological Press, 1984, pp. 24–26. [Online]. Available: <http://img.sslibrary.com/n/slib/book/slib/10103883/48a29d516a9240c6b6ac612136a1f06e/0737a8e073157246fa519fd4d400c759.s>
- [31] C. G. O. I. O. Geology and A. Sinica, "The computation theoretical values of earth tides and its application," *Scientia Geologica Sinica*, vol. 3, pp. 246–268, Aug. 1974.
- [32] *Technical Standard for DC Interference Mitigation of Buried Pipeline*, Standard GB 50991-2014, Ministry of Housing and Urban-Rural Development of the People's Republic of China (MOHURD) & State Administration for Market Regulation, China, 2014.
- [33] C.-M. Liu, "Mid-low latitude power grid geomagnetically induced currents and its assessing method," Ph.D. dissertations, Dept. Elect. Eng., North China Electr. Power Univ., Beijing, China, 2009.



ZEBANG YU was born in Songyuan, China, on April 20, in 1989. He received the B.S. degree in Automation Specialty from the Institutes of Technology of Tianjin in 2012 and the M.S. degree in electrical engineering from Northeastern University, Shenyang, China, in 2014, and he is currently pursuing the Ph.D. degree in electrical engineering from North China Electric Power University, Beijing, China. Since 2015, he has been working on conduction research with the State Key Laboratory of Alternate Electrical Power System with Renewable Energy Sources, North China Electric Power University, Beijing. His research interests include control and analysis in power system operation, power system monitoring and mitigation, modeling geomagnetically induced currents in the oil and gas pipelines, and assessing the effect on buried pipeline systems.



XUAN WANG received the B.S. degree from the Hebei University of Technology, China, in 2014. She is currently pursuing the Ph.D. degree with the School of Electrical and Electronic Engineering, North China Electric Power University, Beijing, China. Her research interests include the risk assessment of magnetic storm, and prevention and control of power grid disaster.



LIANGUANG LIU was born in Jilin Province, China, in 1954. He received the M.Sc. degree in electrical engineering from North China Electric Power University (NCEPU), Beijing, China, in 1994. He has been a Professor and a Doctoral Supervisor at the School of Electrical and Electronic Engineering, NCEPU. His research interests include safe operation and hazard prevention of power systems and power quality. Prof. Liu is a Senior Member of the Chinese Society for Electrical Engineering. He is a Commissioner of the Chinese Space Weather Committee and National Space Weather Monitoring and Prevention Technology Standard Committee.



WENLIN LIU was born in Beijing, China, in 1981. He received the B.S. degree from the North China Electric Power University (NCEPU). He is currently working with Tianhe Benan Electric Power Technology Co., Ltd. in Dezhou. He is mainly engaged in the design and development of monitoring devices for electromagnetic interference in power grids, and oil and gas pipelines.

...